

RESEARCH PAPER

Structural and Optical Properties of Sr-Modified Bismuth Silicate Nanostructured Films Synthesized by Sol Gel Method

Saeid Hajjafari-Bidgoli, Abbas Sadeghzadeh-Attar * and Mohammad Reza Bafandeh

Department of Metallurgy and Materials Engineering, University of Kashan, Kashan, Iran.

ARTICLE INFO

Article History:

Received 01 July 2017

Accepted 22 September 2017

Published 01 October 2017

Keywords:

$\text{Bi}_4\text{Si}_3\text{O}_{12}$

Nanostructured coat

Optical properties

Strontium

Structural properties

ABSTRACT

In this work, the effects of strontium addition on the structure and optical properties of nanostructured bismuth silicate ($\text{Bi}_4\text{Si}_3\text{O}_{12}$) thin films prepared via sol-gel were studied. At first, different sols containing the optimum ratio of precursors were synthesized, and then, the prepared sols were coated on the substrate via dip coating. The dip coated samples were dried at 100°C and, in order to obtain the crystalline structure, calcination was done at 700°C for 1 h. The prepared thin films were characterized and analyzed via scanning electron microscope (SEM), energy dispersive spectroscopy (EDS), atomic force microscope (AFM), and X-ray diffraction (XRD) analyses as well as ultraviolet-visible spectroscopy. The results showed that a homogeneous coating of bismuth silicate with the grain size in the range 35-50 nm could be formed. XRD analysis demonstrated the annealed sample at 700°C composed of crystalline $\text{Bi}_4\text{Si}_3\text{O}_{12}$ phase without any secondary phase. Investigation of the optical properties of the prepared thin films revealed that the addition of strontium decreased transparency from 82 to 78% and band gap from 3.61 to 3.32 eV.

How to cite this article

Hajjafari Bidgoli S, Sadeghzadeh Attar A, Bafandeh M. R. Structural and Optical Properties of Sr-Modified Bismuth Silicate Nanostructured Films Synthesized by Sol Gel Method. J Nanostruct, 2017; 7(4):258-265.

INTRODUCTION

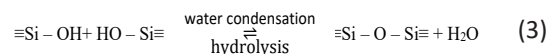
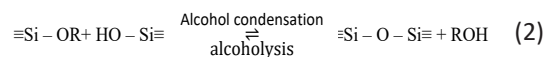
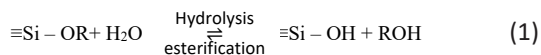
Bismuth silicate ceramics have piezoelectric properties, optical activity, photoconductivity, and photorefractive properties which make them attractive in the applications such as optical devices, optical laser, and ferroelectric memories [1-4]. $\text{Bi}_4\text{Si}_3\text{O}_{12}$ is a ferroelectric material with many applications due to its low dielectric permittivity, high Curie temperature, and spontaneous polarization [5-8]. This material is also used as a buffer layer for the growth of oxide layer on Si [9]. Moreover, $\text{Bi}_4\text{Si}_3\text{O}_{12}$ is transparent in both the visible and near-IR regions, which makes it an attractive candidate for diode pumped

microchip lasers [10]. The formula of bismuth silicate is $\text{Bi}_x\text{Si}_y\text{O}_z$, which is abbreviated as BSO. There are some crystalline compounds in Bi_2O_3 - SiO_2 system. Ternary bismuth silicate compounds are composed of different phases such as Bi_2SiO_5 , $\text{Bi}_4\text{Si}_3\text{O}_{12}$ and $\text{Bi}_{12}\text{SiO}_{20}$ [5-8]. $\text{Bi}_4\text{Si}_3\text{O}_{12}$ (BSO) phase is known as eulytite and its structure is similar to that of $\text{Bi}_4\text{Ti}_3\text{O}_{12}$ [11]. $\text{Bi}_4\text{Ti}_3\text{O}_{12}$ has the perovskite structure, in which triple Ti-O octahedral is placed between $(\text{Bi}_2\text{O}_2)^{2+}$ layers [12-14]. BSO thin films have been prepared successfully via different methods such as chemical vapor deposition [15], sol-gel [2, 16], and pulse laser deposition [17, 18]. Among these methods, sol-gel process is

* Corresponding Author Email: sadeghzadeh@kashanu.ac.ir

considered as a feasible method for preparing thin films for electronic and optical applications. The main advantages of sol-gel technique for the preparation of nanomaterials are the possibility for fabrication complex and homogeneous compounds, low temperature of processing, low cost, versatility, and flexible rheology allowing easy shaping and embedding. They offer unique opportunities for access to organic-inorganic materials [19, 20]. This method makes it possible to obtain doped films, which permits varying their physical properties (electrical conductivity, photoconductivity, optical absorption spectra, and others) purposefully. The main obstacle to using the sol-gel method is the complexity of the chemical process, due to the multicomponent nature of the composition [21].

Sol-gel chemistry is based on inorganic polymerization reactions, which allow the synthesis of ceramic materials with a high degree of homogeneity. This is due to the mixing of the metallic precursors at the molecular level in the solution. Silicate compounds are most often synthesized by hydrolysis and condensation reactions of alkoxide precursors by employing a mineral acid as a catalyst. The most commonly used precursors of oxides are alkoxides due to their commercial availability and high ability of the M-OR bond which could facilitate in situ tailoring during processing. The polymerization starts with the hydroxylation of alkoxide precursors through the hydrolysis of the alkoxy group, which is then followed by the polycondensation reaction (oxolation, ololation). The hydrolysis, oxolation and ololation reactions are involved in the transformation of a molecular alkoxide precursor into an oxide network. At the functional group level, three reactions are generally used to describe the sol-gel method [22]:



where R is an alkyl group, $\text{C}_x\text{H}_{2x+1}$. In the hydrolysis reaction, alkoxide groups (OR) are replaced with a hydroxyl group (OH) and condensation reactions involving the silanol groups subsequently produce siloxane bonds (Si-O-Si). The different cations are

uniformly distributed on an atomic scale through M-O-M bridges. However, some problems exist in the formation of homogeneous multi-component solution, one of which is the unequal hydrolysis and condensation rates of the metal alkoxides. This can result in phase separation, during the hydrolysis and heat treatment and lead to higher crystallization temperature or even undesired crystalline phases [23]. There are different methods such as dip coating, spin coating, and spraying for the preparation of thin films from precursor solutions. In the dip coating method, the substrate is immersed in the precursor solution and, then, withdrawn at a constant rate. During the deposition of the thin film on the substrate, the evaporation of the solvent and the condensation take place simultaneously. The microstructure of coating is determined based on the competition between the evaporation of the solvent and the condensation. Compared with the other methods for the preparation of thin films, the sol-gel dip coating requires considerably less equipment and non-vacuum facilities; therefore, it is less expensive. However, the most important advantage of sol-gel over conventional coating methods is the ability to tailor the microstructure of the deposited films [24].

In this study, the nanostructured bismuth silicate ($\text{Bi}_4\text{Si}_3\text{O}_{12}$) thin films were prepared via sol-gel dip coating and the effect of strontium addition on the structure, morphology, and optical properties was studied.

MATERIALS AND METHODS

Synthesis of bismuth silicate nanostructured films

In order to prepare bismuth silicate gel, firstly, bismuth nitrate pentahydrate (Sigma Aldrich, 99.99% purity) was dissolved in acetic acid and deionized water as solvents according to Table 1. The mixing was done by a stirrer at room temperature for 30 min. On the other hand, the solution of tetra ethylortho silicate (TEOS) in ethanol and acetylacetone was prepared. This solution was added to the first one and mixed at room temperature for 60 min in order to obtain a fully transparent sol. For the preparation of bismuth silicate-strontium sol, in addition to the above steps, a solution containing strontium acetate, acetic acid, and deionized water was prepared. This solution was added to the former solutions and resulted in a transparent stable sol. The prepared sols were coated on the glass slide

Table 1. Molar ratio of used materials for the preparation of different sols.

Sample	TEOS	bismuth nitrate pentahydrate	acetylacetonate	acetic acid	ethanol	deionized water	strontium acetate
BSO	3	4	3	60	120	360	0
BSS1	3	3	3	60	120	360	1
BSS2	3	2	3	60	120	360	2
BSS3	3	1	3	60	120	360	3

via dip coating at the rate of 1 mm/s. The coated samples were dried at 100 °C, and in order to obtain the crystalline structure, calcination was done at 700 °C for 1 h.

Characterization of nanostructured films

Fourier transformation infrared (FTIR) device (TENSOR 27 model) was used in order to determine functional groups in the samples (from 400-4000 cm^{-1}). Phase analysis was performed using an X-ray diffractometer (XRD, X'pert PRO MRD, Philips) using Cu K α radiation ($\lambda=1.542 \text{ \AA}$) at the operating voltage and current of 40 kV and 30 mA, respectively through $2\theta=20-80^\circ$. Morphology, shape, and size of the prepared films were studied by scanning electron microscopy (LEO 1450 VP) and their composition was determined using an energy dispersive X-ray (EDX) microanalyzer coupled to the microscopy. A thin layer of gold

was coated on the surface of the samples in order to make them conductor. Atomic force microscopy (DS 95-50E) was used to study the surface morphology of the films. Optical properties of the films were investigated by UV-Vis spectrometer (Unicam) within the range 300-800 nm. The photoluminescence (PL) spectra were measured by a Hitachi, F-4500 fluorescence spectrophotometer in the range 300-600 nm. A Xe lamp with a filter was used as the excitation light source.

RESULTS AND DISCUSSION

Microstructure of thin films

Fig. 1 shows the SEM images of annealed BSO, BSS1, BSS2, and BSS3 samples at 700 °C for 1 h. As could be seen, the particles were almost spherical and their size was in the range of 35-50 nm. Addition of strontium to bismuth silicate resulted in particle size reduction. This reduction could be attributed

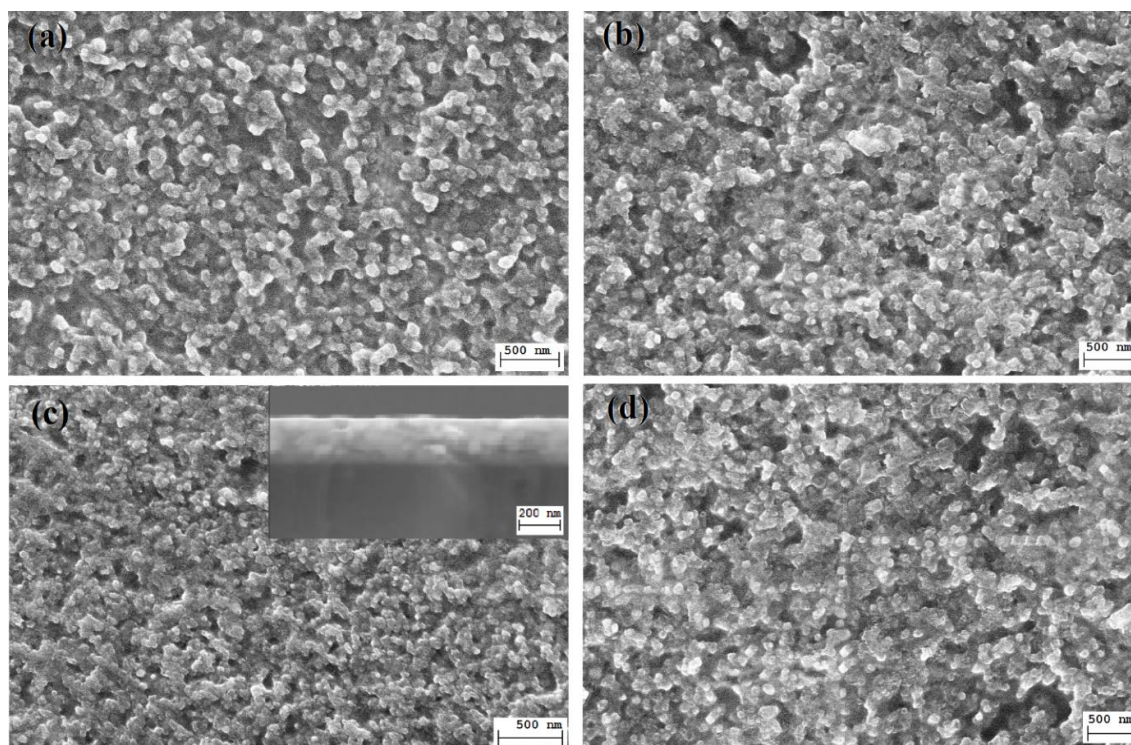


Fig. 1. SEM images of (a) BSO, (b) BSS1, (c) BSS2; the inset shows the cross section, and (d) BSS3 thin films annealed at 700°C for 1h.

to the increase of point defects due to strontium addition and, consequently, movement of grain boundaries became more difficult. As a result, grain growth was hindered. The presence of strontium at grain boundaries was another mechanism which prevented grain growth [25]. According to Fig. 1, the films were dense and, in some regions, consisted of asymmetric agglomerated grains so that one large grain was composed of many smaller grains. This observation could be due to the nature of sol gel process. Another factor which was responsible for agglomeration was annealing the samples at relatively high temperature for a long time, which enhanced diffusion and consequently, grain growth [26]. On the other hand, if the samples were soaked for a shorter time, crystallization could not be completed. Therefore, the selection of proper soaking time and temperature to complete crystallization is so important. Due to the agglomeration of grains, their shapes are completely asymmetric. In Fig. 1c, the cross-section of BSS2 nanostructured layer is shown. As can be observed, the thickness of this layer was in the range 150 to 180 nm. The results

of EDS analysis of different samples are shown in Fig. 2, in which Bi, Si, and O elements were present in BSO sample (Fig. 2a). Based on Figs. 2b to 2d, the presence of Sr beside Bi, Si, and O elements could be seen. According to Table 2, the addition of Sr was accompanied by the reduction of weight percentage of Bi and increment of weight percentage of Si and O.

AFM analysis

AFM images of annealed thin films at 700°C for 1 h are shown in Fig. 3. Figs. 3a and 3b demonstrate 3D and 2D views of bismuth silicate-strontium nanostructures, respectively. As can be seen in the AFM images, surface of the thin film was relatively smooth, crack-free, and homogeneous. The thickness of this layer varied from 150 to 180 nm.

XRD analysis

XRD patterns of different samples are shown in Fig. 4. XRD pattern of BSO sample (Fig. 4a) exhibited peaks at $2\theta=21.3, 27.5, 32.8, 35, 43.2, 45, 52, \text{ and } 55.1^\circ$, which were in agreement with (211), (310), (321), (400), (422), (431), (530), and

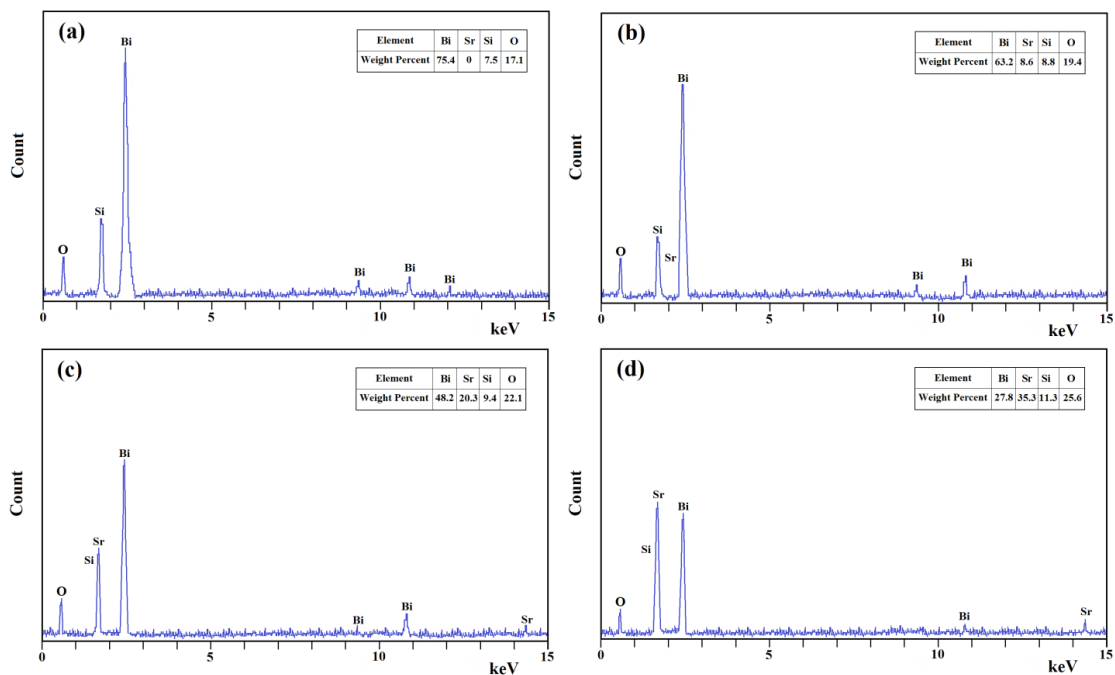


Fig. 2. EDS analyses of (a) BSO, (b) BSS1, (c) BSS2 and (d) BSS3 thin films.

Table 2. Mean crystallite size of different thin films.

Sample	BSO	BSS1	BSS2	BSS3
Mean crystallite size (nm)	22	20	15	18



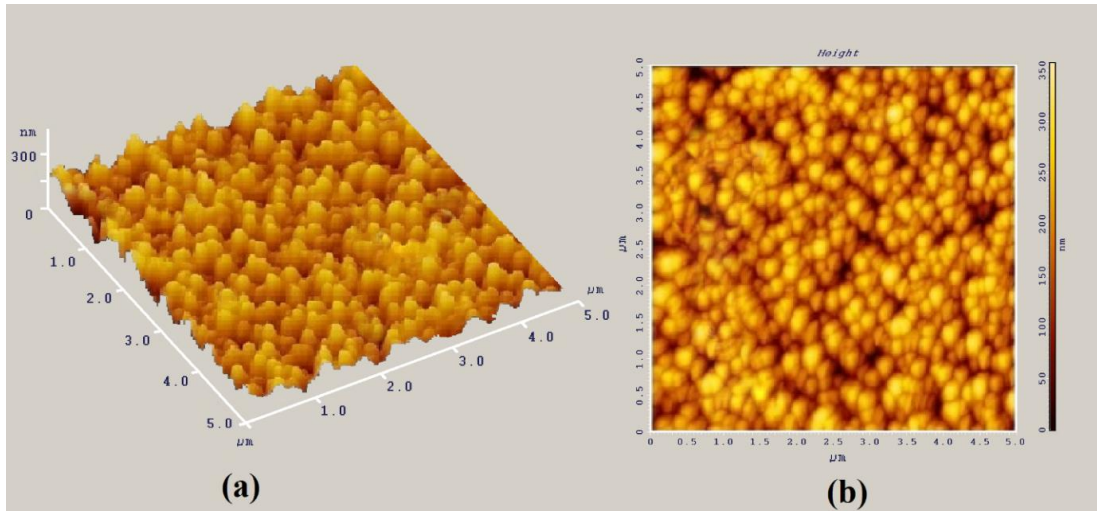


Fig. 3. (a) 3-D and (b) 2-D AFM images of the surface of BSS2 thin film.

(532) planes, respectively. Comparing this pattern with JCPDS 33-0215 pattern proved the formation of cubic $\text{Bi}_4\text{Si}_3\text{O}_{12}$ phase with lattice parameter $a=10.291 \text{ \AA}$ without any secondary phase. Sample

BSS1 (Fig. 4b) showed the related peaks to crystalline $\text{Bi}_6\text{Sr}_2\text{O}_{11}$ phase besides $\text{Bi}_4\text{Si}_3\text{O}_{12}$ peaks as the main phase. Intensities of $\text{Bi}_4\text{Si}_3\text{O}_{12}$ peaks in BSS1 sample were lower than those of BSO

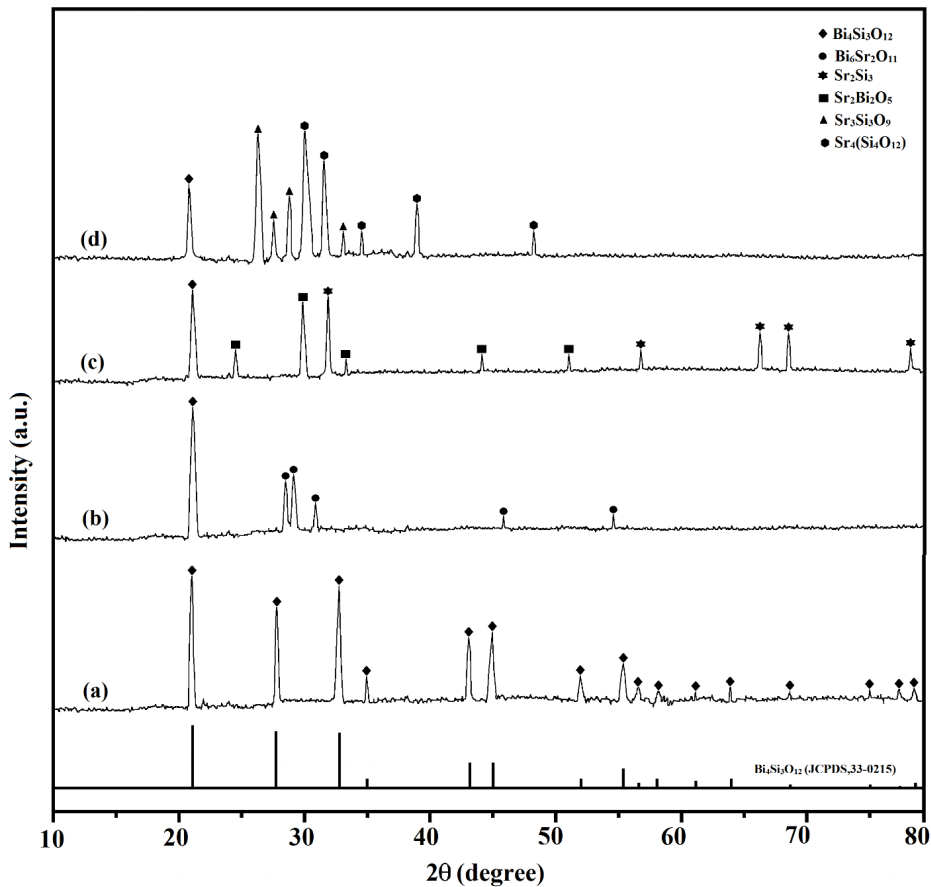


Fig. 4. XRD patterns of (a) BSO, (b) BSS1, (c) BSS2 and (d) BSS3 thin films.

sample. In Fig. 4c which shows the XRD pattern of BSS2, some peaks related to crystalline $\text{Bi}_2\text{Sr}_2\text{O}_5$ and Sr_2Si_3 could be seen beside $\text{Bi}_4\text{Si}_3\text{O}_{12}$ peaks. The intensity of $\text{Bi}_4\text{Si}_3\text{O}_{12}$ peaks as the main phase was reduced in BSS2 compared with BSS1. XRD pattern of BSS3 sample (Fig. 4d) consisted of the related peaks to $\text{Bi}_4\text{Si}_3\text{O}_{12}$ as the main phase as well as $\text{Sr}_4(\text{Si}_4\text{O}_{12})$ and $\text{Sr}_3\text{Si}_3\text{O}_9$ as secondary phases. The intensity of $\text{Bi}_4\text{Si}_3\text{O}_{12}$ peaks in BSS3 was lower than that of BSS2 one. Due to the dependence of properties of synthesized films on their crystallite size, Scherrer's equation [27] was used to calculate the crystallite size of the samples:

$$D = 0.9 \lambda / \beta \cos \theta \quad (4)$$

where D is crystallite size, β is full width at half maximum (FWHM) of the peak, λ is wavelength of the used X-ray, and θ is diffraction angle. FWHM

was determined using X'Pert HighScore software and the calculated crystallite sizes for different samples are listed in Table 2. The results in Table 2 were in good agreement with the XRD patterns of the samples. According to Fig. 4, increase of Sr amount resulted in peak broadening and reduction of their intensities. Therefore, it could be concluded that Sr addition results in grain size reduction. This observation is due to the precipitation of Sr in grain boundaries through crystallization, which hinders grain growth. On the other hand, the precipitated Sr particles into grain boundaries are suitable sites for the nucleation of new grains. As a result, the number of grains increased and their size decreased [25].

UV-Visible absorption spectroscopy

Transmittance spectra and Tauc band gap of

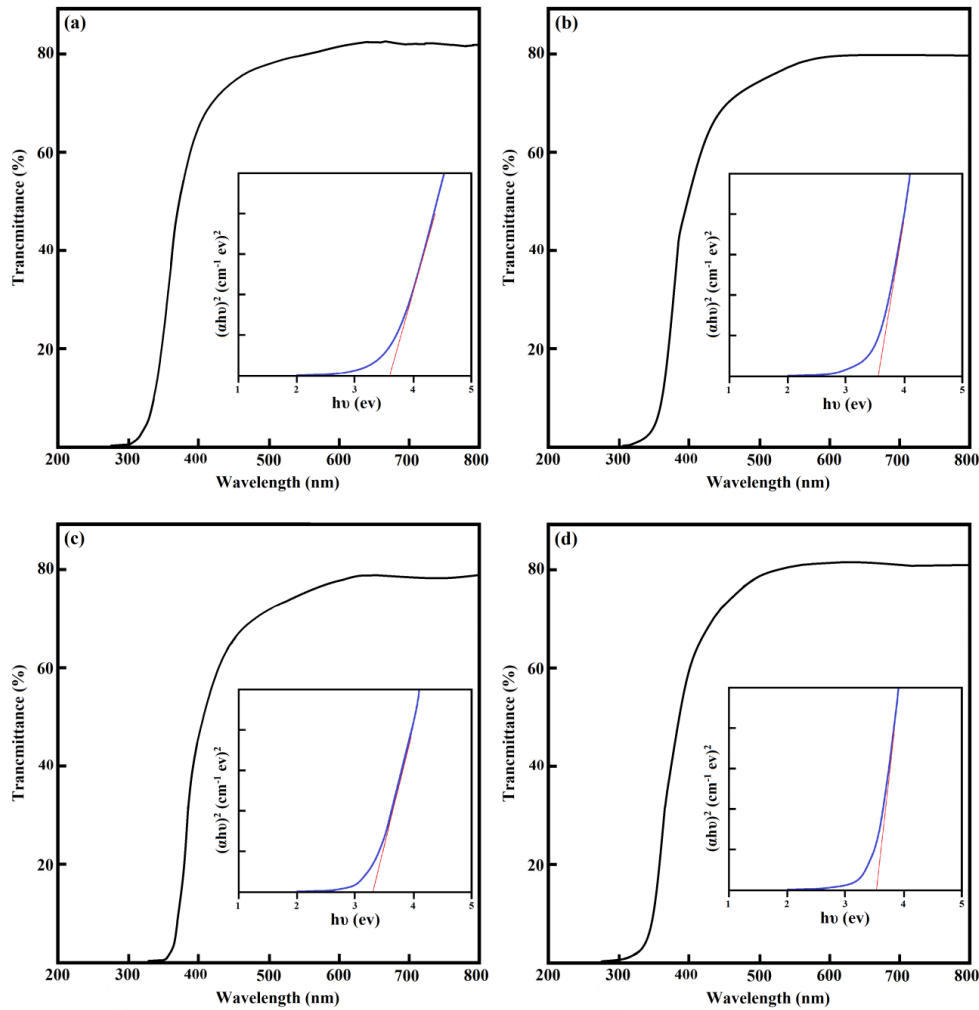


Fig. 5. Transmittance spectra and band gap of (a) BSO, (b) BSS1, (c) BSS2 and (d) BSS3 thin films.

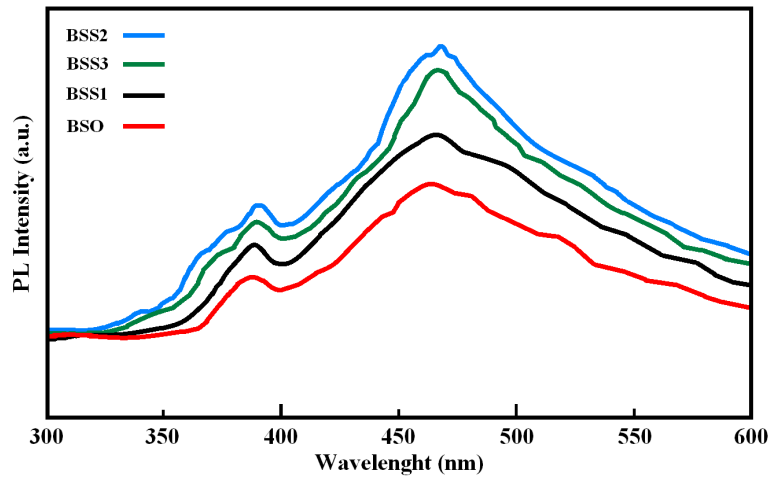


Fig. 6. Photoluminescence spectra of BSO, BSS1, BSS2, and BSS3 thin film.

thin films are shown in Fig. 5. According to this figure the addition of Sr reduced the transparency of bismuth silicate [28]. Transparency of BSO thin film is about 82% and reduced to 78% for BSS2 thin film. Band gap could be estimated from the absorption coefficient (α). Absorption coefficient was calculated according to the following equation [29]:

$$\alpha = 2.303 A/t \quad (5)$$

where A is absorption and t is thickness of the sample. Relation between α and energy of photon ($h\nu$) is expressed by [30]:

$$\alpha = B(h\nu - E_g)^2/h\nu \quad (6)$$

where B is a constant and E_g is band gap. The above equation could be written as:

$$(\alpha h\nu)^{\frac{1}{2}} = B(h\nu - E_g) \quad (7)$$

The latter equation is known as Tauc relation and is used to calculate band gap. Tauc relation is expressed generally as [31]:

$$(\alpha h\nu)^n = B(h\nu - E_g) \quad (8)$$

The exponent n equals 2 for direct allowed transitions and equals 1/2 for indirect allowed transitions. Bismuth silicate possesses direct allowed transitions, so its exponent is n=2. By drawing $(\alpha h\nu)^2$ versus incident photon energy ($h\nu$) and extrapolation of its linear region, band gap (E_g) could be estimated. Band gap of different thin films are shown in Fig. 5. It could be seen that, by the addition of Sr, band gap was reduced and moved toward wavelengths with less energy. Band gap for BSO, BSS1, BSS2, and BSS3 was calculated

as 3.61, 3.56, 3.32, and 3.53 eV, respectively.

Luminescent analysis

Fig. 6 shows the emission spectrum of BSO, BSS1, BSS2, and BSS3 samples, which was monitored with the excitation wavelength of 260 nm. A broad band signal emitted with the maximum intensity at about 470 nm was obtained. The measured emission bands at 470 nm could be properly attributed to the electronic transitions of 6p→6s [32]. Moreover, luminous intensity increased with the addition of Sr. The observed changes in luminous intensity can be mainly resulted from the grain growth and improvement of crystal perfection due to the addition of Sr. As can be seen, BSS2 sample showed the highest luminous intensity among the other samples.

CONCLUSION

Nanostructured bismuth silicate thin films were prepared successfully and the effects of Sr addition on the structure, morphology, and optical properties were investigated. SEM images showed the formation of homogeneous coating with the size in the range of 35-50 nm, which was in good agreement with the results obtained from Scherrer's equation based on the width of XRD peaks. Therefore, the addition of strontium to $\text{Bi}_4\text{Si}_3\text{O}_{12}$ decreased grain size. XRD pattern of the annealed samples demonstrated the formation of crystalline $\text{Bi}_4\text{Si}_3\text{O}_{12}$ phase without any secondary phase. Moreover, the addition of strontium decreased transparency and band gap of the prepared thin films.

CONFLICT OF INTEREST

The authors declare that there are no conflicts of interest regarding the publication of this manuscript.

REFERENCES

1. Lira CA, Ramirez MO, Garcia Sole J, Caldino U. Photoluminescence of $\text{Bi}_4\text{Si}_3\text{O}_{12}:\text{Er}^{3+}$ crystal excited in the commercial laser diode emission region. *Opt. Mater.*, 2007; 29(6): 605-9.
2. Gunter P. Holography, coherent light amplification and optical phase conjugation with photorefractive materials. *Phys. Rep.*, 1982; 93(4): 199-299.
3. Mosquera L, Oliveira I, Frejlich J, Hernandez AC, Lanfredi S, Carvalho JF. Dark conductivity, photoconductivity, and light-induced absorption in photorefractive sillenite crystals. *J. Appl. Phys.*, 2001; 90(6): 2635-41.
4. Burkov VI, Kargin YF, Volkov VV, Zubovich NY. Spectroscopic and chiroptical properties of doped sillenite crystals. I. absorption and circular-dichroism spectra of $\text{Bi}_{12}\text{SiO}_{20}$ and $\text{Bi}_{12}\text{TiO}_{20}$ crystals doped with phosphorus and vanadium. *Inorg. Mater.*, 1994; 30: 997-1001.
5. Klebansky EO, Kudzin AY, Pasalskii VM, Plyaka SN, Sadovskaya LY, Sokolyanskii GK. Thin sol-gel bismuth silicate films. *Phys. Solid State*, 1999; 41(6): 913-5.
6. Yamaguchi M, Nagatomo T, Masuda Y. Preparation of $\text{Bi}_4\text{Ti}_3\text{O}_{12}/\text{Bi}_2\text{SiO}_5/\text{Si}$ structures derived by metal organic decomposition technique. *Jpn. J. Appl. Phys.*, 2001; 40(9B): 5559-63.
7. Sun S, Lu P, Fuierer PA. Oriented bismuth titanate thin films by single-solid-source metal-organic chemical vapour deposition. *J. Cryst. Growth*, 1999; 205(1): 177-84.
8. Wills LA, Feil WA, Wessels BW, Tonge LM, Marks TJ. Growth studies of ferroelectric oxide layers prepared by organometallic chemical vapor deposition. *J. Cryst. Growth*, 1991; 107(1-4): 712-5.
9. Kim J, Tsurumi T, Kamiya T, Daimon M. Growth of bismuth silicate films on Si and its dielectric properties. *J. Appl. Phys.*, 1994; 75(6): 2924-8.
10. Sato Y, Shoji I, Kurimura S, Taira T, Senguttuvan N, Ishii M, Koboyashi M. Optical absorption and emission spectroscopy of $\text{Nd}:\text{Bi}_4\text{Si}_3\text{O}_{12}$ grown by Bridgeman method. *Adv. Solid State Lasers*, 2001; 50: 67-71.
11. Yamaguchi M., Hiraki K, Homma T, Nagatomo T, Masuda Y. Fabrication and properties of Bi_2SiO thin films for MFIS structures. *IEEE International Symposium on Application of Ferroelectrics*, 2001; 12: 629-32.
12. Fouskova A, Cross LE. Dielectric properties of bismuth titanate. *J. of Appl. Phys.*, 1970; 41(7): 2834-8.
13. Scott JF, Paz de Araujo CA, Melnick BM. Loss mechanisms in fine-grained ferroelectric ceramic thin films for ULSI memories (DRAMs). *J. Alloys Compd.*, 1994; 211: 451-4.
14. Takenaka T, Sakata K. Grain orientation effects on electrical properties of bismuth layer structured ferroelectric $\text{Pb}_{1-x}(\text{Na,Ce})_{x/2}\text{Bi}_2\text{Ti}_4\text{O}_{15}$ solid solution. *J. Appl. Phys.*, 1984; 55(4): 1092-9.
15. Nagao YN, Mimura Y. Epitaxial growth of $\text{Bi}_{12}\text{SiO}_{20}$ films by chemical vapor deposition. *Jpn. J. Appl. Phys.*, 1985; 24(12): 954-5.
16. Wei Q, Liu G, Zhou Z, Yang H, Zhuang J, Liu Q. Luminescence behaviors of a novel white-emitting phosphor $\text{Bi}_4\text{Si}_3\text{O}_{12}:\text{Dy}$ prepared via sol-gel route. *J. Lumin.*, 2014; 145: 803-7.
17. Alonso JC, Diamant R, Poniatowski EH, Guasti MF, Munoz G, Camarillo I, Jouanne M, Morhange JF. Raman characterization of $\text{Bi}_{12}\text{SiO}_{20}$ thin films obtained by pulsed laser deposition. *Appl. Surf. Sci.*, 1997; 109-110: 359-61.
18. Okada T, Yahiro F, Uetsohara H, Nakata Y, Maeda M, Higuchi S. Deposition of highly oriented $\text{Bi}_{12}\text{SiO}_{20}$ thin films on Y-stabilized zirconia and SiO_2 by pulsed-laser deposition. *Appl. Phys.*, 1999; 69(Suppl 1): 723-6.
19. Thanabodeekij N, Gulari E, Wongkasemjit S. $\text{Bi}_{12}\text{TiO}_{20}$ synthesized directly from bismuth (III) nitrate pentahydrate and titanium glycolate and its activity. *Powder Technol.*, 2005; 160(3): 203-8.
20. Pierre AC. Introduction to sol-gel processing. Springer Science + Business Media, New York, USA, 1998.
21. Owens G, Singh RK, Foroutan F, Alqaysi M, Han CM, Mahapatra C, Kim HW, Knowles JC. Sol-gel based materials for biomedical applications. *Prog. Mater Sci.*, 2016; 77: 1-79.
22. Brinker CJ, Scherer GW. Sol-gel science; the physics and chemistry of sol-gel processing. Academic Press, INC, 1989.
23. Veber A, Kunej SP, Suvorov D. Synthesis and microstructural characterization of $\text{Bi}_{12}\text{SiO}_{20}$ (BSO) thin films produced by the sol-gel process. *Ceram. Int.*, 2010; 36(1): 245-50.
24. Brinker CJ, Frye GC, Hurd AJ, Ashley CS. Fundamentals of sol-gel dip coating. *Thin Solid Films*, 1991; 201(1): 97-108.
25. Gao L, Zhai J, Yao X. The influence of Co doping on the dielectric, ferroelectric and ferromagnetic properties of $\text{Ba}_{0.70}\text{Sr}_{0.30}\text{TiO}_3$ thin films. *Appl. Surf. Sci.*, 2009; 255(8): 4521-5.
26. Chaim R, Levin M, Shlayer A, Estournes C. Sintering and densification of nanocrystalline ceramic oxide powders: a review. *Adv. Appl. Ceram.*, 2008; 107(3): 159-169.
27. Cullity BD. Elements of X-ray diffraction. Addison Wesley pub., Menlo Park, CA, USA, 1978.
28. Zhou YF, Wang JC, Tang LA, Pan ZL, Chen NF, Chen WC, Huang YY, He W. Space growth studies of Ce-doped $\text{Bi}_{12}\text{SiO}_{20}$ single crystal. *Mater. Sci. Eng. B*, 2004; 113(3): 179-83.
29. Dimitrov V, Komatsu T. Classification of oxide glasses: a polarizability approach. *J. Solid State Chem.*, 2005; 178(3): 831-46.
30. Lee S, Hwang S, Cha M, Shin H, Kim H. Role of copper ion in preventing silver nanoparticles forming in $\text{Bi}_2\text{O}_3\text{-B}_2\text{O}_3\text{-ZnO}$ glass. *J. Phys. Chem. Solids*, 2008; 69(5-6): 1498-500.
31. Wood DL, Tauc J. Weak absorption tails in amorphous semiconductors. *Phys. Rev. B: Condens. Matter B*, 1972; 5(8): 3144-51.
32. Sokolov VO, Plotnichenko VG, Dianov EM. The origin of near-IR luminescence in bismuth-doped silica and germania glasses free of other dopants: first-principle study. *Opt. Mater. Express*, 2013; 3(8): 1059-74.